DOI: 10.1021/ma100006x

Macromolecules
ARTICLE

Crystalline Random Conjugated Copolymers with Multiple Side Chains: Tunable Intermolecular Interactions and Enhanced Charge Transport and Photovoltaic Properties

Pei-Tzu Wu,[†] Guoqiang Ren,[†] and Samson A. Jenekhe*[,†,‡]

[†]*Department of Chemical Engineering and* [‡]*Department of Chemistry, University of Washington, Seattle, Washington 98195-1750*

Received January 3, 2010; Revised Manuscript Received February 28, 2010

ABSTRACT: Random poly(3-butylthiophene-*co*-3-octylthiophene) of several compositions were synthesized and found to be highly crystalline in spite of the statistical arrangement of the different-sized side chains. The melting (T_m) and recrystallization (T_c) temperatures of the random copolythiophenes varied continuously with composition. The interlayer d_{100} stacking distance in the lamellar crystalline structure of the random copolymers, determined from X-ray diffraction of films, varied linearly with copolymer composition over the entire range. Fullerene-based bulk heterojunction solar cells made from the random copolythiophenes had power conversion efficiencies of up to 3.0% under 100 mW/cm^2 AM1.5 illumination in air, which is significantly enhanced compared to the homopolymers and their physical blends. The space charge limited current mobility of holes in the random copolythiophenes was enhanced compared to poly(3-butylthiophene) and physical blends of the homopolymers. Transmission electron microscopy images of the bulk heterojunction thin films showed that the random copolythiophenes had a worm-like nanoscale phase-separated morphology beneficial to solar cells. These results demonstrate that random copolymerization and multiple-sized side chains provide a facile means of fine-tuning the structural and electronic/optoelectronic properties of conjugated polymers. The results also provided new insights on the lamellar crystalline packing of side-chain bearing conjugated polymers.

Introduction

Many conjugated polymers such as polythiophenes,[1] poly(*p*-phenylene)s,[2] poly(arylene vinylene)s,[3] poly(arylene ethynylene)s,[4] polypyrroles,[5] polyfluorenes,[6] polycarbazoles[7] (shown in Chart 1), polyquinolines,[8] and polyquinoxalines[9] carry nonconjugated side chains (e.g., alkyl and alkoxyl groups) that improve solubility of the rigid rod-like polymer backbones in organic solvents, modulate intermolecular interactions, and facilitate ordered packing in the solid state.[1−10] The insulating side chains play an important role not only in the structural and physical properties (e.g., solubility, morphology, and thermal properties) but can also greatly affect the electronic and optoelectronic properties of the conjugated polymers.[11,12] In the solid state, all such side-chain bearing conjugated polymers (Chart 1), if regioregular or regiosymmetric, generally form a lamellar crystalline structure, where the interlayer stacking distance is determined by the length or size of the side chain.[1−9] Among consequences of the magnitude of the interlayer stacking distance is that while longer alkyl side chains increase solubility and lower the melting temperature, they can also result in less efficient charge transport as exemplified by the poly(3-alkylthiophene)s (P3ATs).[13]

The lamellar crystalline structure of conjugated polymers with regioregular or regiosymmetric side chains, is known to depend on the side-chain density, the presence of side-chain interdigitation and/or side-chain crystallization.[14−19] Regiosymmetric poly(5,5′-bis(3-dodecyl-2-thienyl)-2,2′-bithiophene) (PQT-12)[15] and poly(2,5-bis(3-alkylthiophene-2-yl)thieno[3,2-*b*]thiophene)s (PBTTTs)[16,17] with a low density of side-chain attachment and uniform side-chain arrangement can allow side-chain interdigitation, and thus promote efficient lamellar stacking with long-range order. However, it is argued that in the case of regiosymmetric poly(2,5-bis(3-dodecyl-5-(3-dodecylthiophen-2-yl)thiophen-2-yl)thiazolo[5,4-*d*]thiazole)s (PTzQT-12), whose side chains are not equally spaced along the π-conjugated backbone, the polymer is not likely to exhibit side-chain interdigitation and undergo side-chain crystallization even though it has a similar lamellar packing structure.[18] Similarly, regioregular poly(3-alkylthiophene)s are known to exhibit a lamellar crystalline packing structure where little or no side-chain interdigitation occurs.[1,14] Thus, there are two different models of how the side chains of conjugated polymers are organized: (i) well-aligned, ordered side chains and (ii) randomly arranged side chains, schematically illustrated in Chart 1, parts b and c, respectively.[16,17] To date, the conjugated polymers known to exhibit a lamellar crystalline structure all carry well-defined repeat units, both regioregular and regiosymmetric, and the side-chain length is identical.[1−9,13−19] On the basis

Chart 1. (a) Conjugated Polymers with Side Chains, (b) Lamellar Packing Structure with Side-Chain Crystallization, and (c) Lamellar Packing Structure with Disordered Side Chains

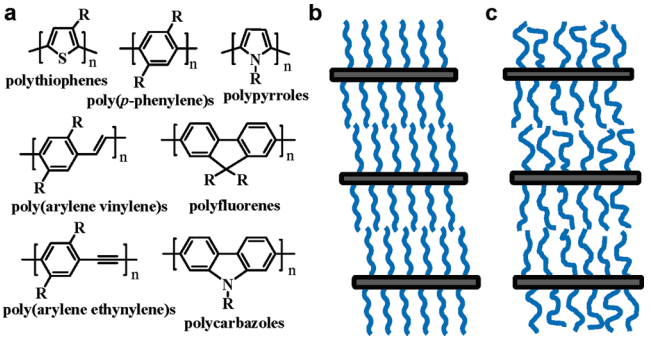

*Author for all correspondence. E-mail: jenekhe@u.washington.edu.

 Published on Web 03/17/2010

Scheme 1. Synthesis of Random Copolymers RBO*x*

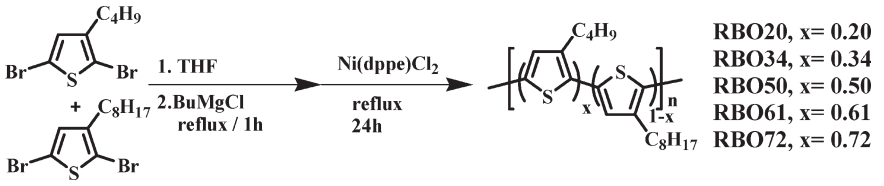

of studies of the lamellar crystalline structure of well-defined homopolymers or AB-type alternating copolymers, it is not clear if side-chain interdigitation, crystallization, or ordered organization are essential to the formation of the lamellar crystalline packing structure.

In this paper, we report the synthesis and studies of the structural and electronic/optoelectronic properties of random poly(3-butylthiophene-*co*-3-octylthiophene)s denoted RBO*x*, where *x* is the copolymer composition in mol % 3-butylthiophene (3BT). We show that the random copolythiophenes melt, crystallize, and self-organize into lamellar crystalline structures similar to their parent poly(3-alkylthiophene)s. Comparative studies of fullerene-based bulk heterojunction (BHJ) solar cells made from the random copolythiophenes showed that their photovoltaic properties were significantly enhanced relative to those of the parent homopolymers or those of the corresponding poly(3-butylthiophene) (P3BT)/poly(3-octylthiophene) (P3OT) physical blends. Measurement of space charge limited current (SCLC) mobility of holes in the BHJ thin films similarly showed enhancement of charge transport in the random copolythiophenes compared to P3BT or the physical blends. We also investigated the morphology of the BHJ thin films of the random copolythiophenes, the homopolymers (P3BT, P3OT), and P3BT/P3OT physical blends by transmission electron microscopy (TEM), providing information on the nanoscale morphology relevant to the performance of the solar cells.

Experimental Section

Materials. 3-Butylthiophene, 3-octylthiophene, *N*-bromosuccinimide (NBS), anhydrous THF, butylmagnesium chloride (BuMgCl, 2 M in THF), and [1,2-bis(diphenylphosphino)ethane]dichloronickel(II) [Ni(dppe)Cl_2] were purchased from Sigma-Aldrich and were used as received. 2,5-Dibromo-3-butylthiophene and 2,5-dibromo-3-octylthiophene were synthesized following the literature method.[20] [6,6]-Phenyl-C_{71} butyric acid methyl ester ($PC_{71}BM$, > 99.0%) and poly(3-butylthiophene) (P3BT, M_n = 107 900 g/mol, PDI = 3.61) were purchased from American Dye Source, Inc. (Quebec, Canada) and used as received. 1,2-Dichlorobenzene (ODCB, anhydrous, > 99%, Aldrich) was degassed with nitrogen before use. Poly(3,4-ethylenedioxythiophene):poly(styrenesulfonate) (PEDOT) (Baytron P VP AI 4083) was purchased from H. C. Stark (Newton, MA), stored in a refrigerator and passed through a 0.45 μm filter before use.

Polymer solutions were prepared by dissolving 20.0 mg of P3BT, P3OT, or random poly(3-butylthiophene-*co*-3-octylthiophene) (RBO*x*, *x* = 20, 34, 50, 61, and 72 mol % 3BT) in 1.0 mL of ODCB with magnetic stirring overnight. The resulting solutions were passed through a 0.45 μm filter (1.0 μm filter in the case of P3BT solution). A series of P3BT/P3OT blends with the same composition (mol % 3BT) as that of RBO*x* was prepared. A 60 mg/mL $PC_{71}BM$ in ODCB was prepared at room temperature and passed through a 0.45 μm filter. To prepare BHJ thin films for photovoltaic devices, a polymer solution (P3BT, P3OT, RBO*x*, or P3BT/P3OT blend) and a $PC_{71}BM$ solution were mixed to make series of BHJ blends with a polymer-to-$PC_{71}BM$ weight ratio of 1:0.75.

Synthesis of Poly(3-butylthiophene-*co*-3-octylthiophene), RBO*x*. A series of poly(3-butylthiophene-*co*-3-octylthiophene) (RBO*x*) was synthesized by a modified Grignard metathesis method (GRIM)[21] as illustrated in Scheme 1. The composition of the series of RBO*x* random copolymers was controlled by varying the feed ratio of 2,5-dibromo-3-butylthiophene and 2,5-dibromo-3-octylthiophene. The typical procedure for the synthesis of RBO*x* copolymers was as follows. A round-bottomed flask (250 mL) equipped with a three-neck stopcock was dried by heating under reduced pressure and cooled to room temperature. 2,5-Dibromo-3-butylthiophene (1 g, 3.36 mmol) and 2,5-dibromo-3-octylthiophene (1.19 g, 3.36 mmol) were placed in the flask under N_2, and then evacuated under reduced pressure to remove any moisture and oxygen inside. After anhydrous THF (35 mL) was added into the flask via a syringe, the solution was stirred at 0 °C. Two M solution of BuMgCl in THF (3.36 mL, 6.72 mmol) was added via a syringe, and the mixture was stirred at 0 °C for 30 min. The solution was then heated up to 50 °C and Ni(dppe)Cl_2 catalyst (24.8 mg, 0.047 mmol) was added in one portion. The resulting solution was stirred at 50 °C overnight. The reaction was quenched by adding HCl solution (20 wt %) into the solution. The crude polymer was successively washed by Soxhlet extraction using methanol, acetone, and hexane. The solvent was removed by evaporation to give a purple solid, RBO50 (0.85 g, Yield: 75%). The ratio of the amount of Ni(dppe)Cl_2 catalyst to the total monomer amount was fixed at 0.7 mol %. RBO20, RBO34, RBO61, and RBO72 with initial (3BT:3OT) molar feed ratios of 20:80, 35:65, 65:35, and 80:20, respectively, were also synthesized in the same manner to give purple solids as the final products. The assignment of each proton resonance in the ^{1}H NMR spectra of RBO*x* samples is as shown in Figure S1 in the Supporting Information.

RBO20 (1.05 g, yield = 57%). ^{1}H NMR ($CDCl_3$), δ (ppm): 7.00 (1H), 2.84−2.59 (2H), 1.74−1.70 (2H), 1.52−1.34 (8.4H), 1.00 (0.6H), 0.89 (2.4H). Regioregularity of RBO20 was determined to be 91.8%.

RBO34 (0.61 g, yield = 52%). ^{1}H NMR ($CDCl_3$), δ (ppm): 7.00 (1H), 2.84−2.59 (2H), 1.74−1.70 (2H), 1.52−1.34 (7.28H), 1.00 (1.02H), 0.89 (1.98H). Regioregularity of RBO34 was determined to be 91.3%.

RBO50 (0.85 g, yield = 75%). ^{1}H NMR ($CDCl_3$), δ (ppm): 7.00 (1H), 2.84−2.59 (2H), 1.74−1.70 (2H), 1.52−1.34 (6H), 1.00 (1.5H), 0.89 (1.5H). Regioregularity of RBO50 was determined to be 94.0%.

RBO61 (0.86 g, yield = 79%). ^{1}H NMR ($CDCl_3$), δ (ppm): 7.00 (1H), 2.84−2.59 (2H), 1.74−1.70 (2H), 1.52−1.34 (5.12H), 1.00 (1.83H), 0.89 (1.17H). Regioregularity of RBO61 was determined to be 92.9%.

RBO72 (0.95 g, yield = 75%). ^{1}H NMR ($CDCl_3$), δ (ppm): 7.00 (1H), 2.84−2.59 (2H), 1.74−1.70 (2H), 1.52−1.34 (4.24H), 1.00 (2.16H), 0.89 (0.84H). Regioregularity of RBO72 was determined to be 90.8%.

P3OT (0.99 g, yield = 88%). ^{1}H NMR ($CDCl_3$), δ (ppm): 7.00 (1H), 2.84−2.59 (2H), 1.74−1.70 (2H), 1.52−1.34 (10H), 0.90 (3H). Regioregularity of P3OT was determined to be 90.8%.

Sample Preparation for X-ray Diffraction. Each copolymer was dissolved in 1,2-dichlorobenzene at 10 mg/mL and the solutions were drop-cast onto glass substrates. The substrates were then dried on a hot plate at 50 °C in air.

Characterization. ^{1}H NMR spectra were recorded on a Bruker-AF300 spectrometer at 300 MHz. UV−visible absorption spectra were recorded on a Perkin-Elmer model Lambda 900

Table 1. Molecular Weight and Thermal/Structural Properties of RBO*x*

copolymer	M_w (g/mol)	M_n (g/mol)	PDI	rr[a] (%)	T_m (°C)	T_c (°C)	ΔH_m (J/g)	d_{100} (Å)
RBO20	112 900	77 800	1.45	91.8	196.1	159.8	15.7	19.5
RBO34	13 100	12 000	1.09	91.3	200.7	164.3	15.4	18.2
RBO50	20 500	15 000	1.36	94.0	216.0	170.6	13.0	16.9
RBO61	11 500	9700	1.18	92.9	211.8	169.8	14.6	16.4
RBO72	9400	8300	1.13	90.8	212.1	174.9	13.1	15.0

[a] Regioregularity.

UV/vis/near-IR spectrophotometer. The photoluminescence (PL) emission spectra were obtained with a Photon Technology International (PTI) Inc. model QM-2001−4 spectrofluorimeter. The molecular weights reported for the polymers were determined on a Polymer Lab gel permeation chromatograph (GPC) Model 120 (DRI, PL-BV400HT Viscometer) against polystyrene standards in chlorobenzene at 60 °C. X-ray diffraction (XRD) patterns were obtained on a Bruker AXS D8 Focus diffractometer with Cu Kα beam (40 kV, 40 mA; $\lambda = 0.15418$ nm). Data were obtained from 2θ angles of 2−35° at a scan rate of 0.01°/s. The d spacing was calculated from the equation, $n\lambda = 2d \sin\theta$. Differential scanning calorimetry (DSC) scans were obtained on TA Instrument Q20 at a heating rate of 10 °C/min.

Fabrication and Characterization of Photovoltaic Cells. Patterned indium tin oxide (ITO) glass substrates (10 Ω/□, Shanghai B. Tree Tech. Consult Co., Ltd., Shanghai, China) were cleaned stepwise by acetone, DI water and isopropyl alcohol in an ultrasonic bath. To fabricate the solar cell devices, a 50 nm PEDOT buffer layer was spin-coated on top of ITO substrate at 3000 rpm for 30 s and dried at 150 °C for 10 min under vacuum. Bulk heterojunction (BHJ) polymer solar cells were fabricated following the basic structure of ITO/PEDOT:PSS/active layer/LiF/Al, where the active layer is a BHJ thin film of P3BT:$PC_{71}BM$, P3OT:$PC_{71}BM$, RBO*x*:$PC_{71}BM$, or P3BT/P3OT blend:$PC_{71}BM$ (1:0.75 w:w). The BHJ blend solution was spin-coated on top of an ITO/glass substrate in a N_2 filled glovebox for 30 s. The as-spun active layers were processed by 30 min film aging and 5 min thermal annealing at (110 ± 10) °C on a hot plate. Additionally, solar cells based on RBO20:$PC_{71}BM$, RBO34:$PC_{71}BM$, and P3OT:$PC_{71}BM$ BHJ thin films were also prepared using a different processing condition (dried at 60 °C for 2 h). The cathode material, consisting of 1.0 nm of LiF and 80 nm of Al was sequentially deposited under vacuum in a thermal evaporator.

Each substrate contained five solar cells with an active area of 4 mm^2. AM1.5 sunlight with 100 mW/cm^2 illumination was simulated by a filtered Xe lamp and calibrated using a NREL calibrated Si diode.[22] All the solar cell characterizations were measured in laboratory ambient air using an HP4155A semiconductor parameter analyzer (Yokogawa Hewlett-Packard, Tokyo).

Space Charge Limited Current Measurement. Devices for space charge limited current (SCLC) measurement were fabricated similar to those of solar cells. The SCLC hole mobility was evaluated using hole-only devices with the structure ITO/PEDOT:PSS/active layer/Au, where the active layer is a BHJ thin film of P3BT:$PC_{71}BM$, P3OT:$PC_{71}BM$, RBO*x*:$PC_{71}BM$, or P3BT/P3OT blend:$PC_{71}BM$ (1:0.75 wt:wt) that was processed under the same conditions as the corresponding solar cells. All the SCLC measurements were done in laboratory ambient air using an HP4155A semiconductor parameter analyzer. The zero-field SCLC hole mobility was obtained by using nonlinear least-squares fitting of the current density−voltage data according to the Mott-Gurney equation[23] (eq 1):

$$J = \frac{9}{8}\varepsilon\varepsilon_0\mu\frac{V^2}{L^3}\exp\left(\frac{0.89\beta}{\sqrt{L}}\sqrt{V}\right) \quad (1)$$

where J is the current density, V is the applied voltage, L is the active layer thickness, μ is the mobility, ε is the relative permittivity, ε_0 is the permittivity of free space, and β is the field-activation factor. The equation is applied under the assumption that the polymer film has good contact with both electrodes and the electrodes sufficiently block electrons from getting to the $PC_{71}BM$. Additional details on these SCLC measurement and analysis can be found in our previous paper.[22]

TEM Imaging. Bright-field transmission electron microscope (BF-TEM) was employed to characterize the morphology of the BHJ thin films directly peeled off the actual solar cells whose photovoltaic properties were measured. To obtain the BHJ thin films, the devices were scratched with a blade and soaked in DI water until the active layers were peeled off the substrates. The BHJ thin films were then supported on TEM grids (400 mesh, Electron Microscopy Sciences) and dried in vacuum. An FEI Tecnai G^2 F20 TEM with 200 kV accelerating voltage was used for imaging, with a 0.031 mm^2 aperture for selected area electron diffraction (SAED). The images were slightly defocused to enhance the phase contrast and were then acquired with a CCD camera and recorded with Gatan DigitalMicrograph software with proper exposure time.

Results and Discussion

Random Copoly(3-alkylthiophene)s. A series of five regioregular poly(3-butylthiophene-*co*-3-octylthiophene)s (RBO*x*, where x is the molar composition of 3-butylthiophene (3BT) units in the copolymer) was synthesized by the GRIM method (Scheme 1).[21] The composition x was determined by using the terminal methyl protons of butyl ($\delta = 1.0$ ppm) and octyl ($\delta = 0.9$ ppm) side chains of RBO*x*. The assignment of the proton resonances in the ^{1}H NMR spectra of RBO*x* are shown in Figure S1 (Supporting Information). The regioregularity of RBO*x* was determined to be 91−94% from the resonance of the α-methylene protons. The random distribution of 3-butylthiophene and 3-octylthiophene in the RBO*x* chains results in good solubility of the copolymers in common organic solvent (e.g., chloroform, chlorobenzene, and 1,2-dichlorobenzene) at high concentrations (~20 mg/mL), facilitating easily solution processing of the materials into thin films.

The number-average molecular weight (M_n) of the RBO*x* samples was in the range of 8300 to 77 800 g/mol, with a polydispersity index of 1.09−1.45, determined by gel permeation chromatography (GPC) analysis against polystyrene standards (Table 1). The M_n values of the five compositions are all in the moderate range except RBO20 (M_n = 77 800) which has a much higher molecular weight. The P3OT sample we synthesized has an M_n of 330 000 g/mol and a PDI of 1.37 whereas the commercially acquired P3BT sample gave an M_n of 107 900 g/mol with a PDI of 3.61 under the same GPC analysis conditions.

The dilute solution (1×10^{-6} to 1×10^{-5} M) absorption spectra of RBO*x*, P3BT and P3OT in toluene are shown in Figure 1a and the corresponding thin-film absorption spectra are shown in Figure 1b. As expected, all the random copolymers and the parent homopolymers have similar absorption spectra with a maximum centered near 450 nm. The thin-film absorption spectra are somewhat structured with long wavelength shoulder peaks at ~525 and 605 nm

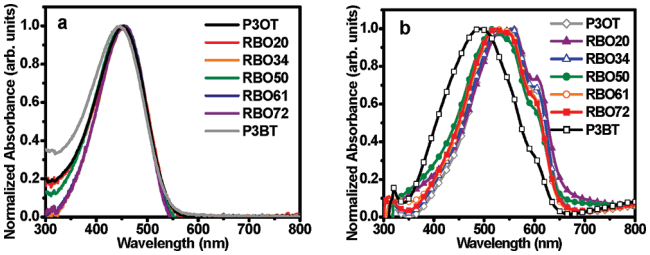

Figure 1. Absorption spectra of RBO*x* copolymers in dilute toluene solution (a) and as thin films (b). The solution and thin-film absorption spectra of homopolymers P3BT and P3OT are also shown.

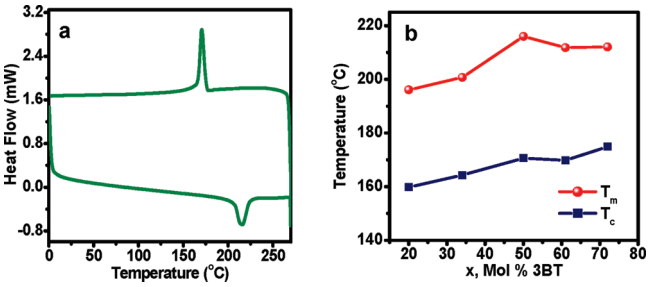

Figure 2. (a) Second heating/cooling DSC scan of RBO50. (b) The compositional (*x*, mol % 3BT) dependence of the melting (T_m) and recrystallization (T_c) transition temperatures of random copolymers RBO*x*.

and absorption maximum that varied from ~520 nm in RBO50, RBO61, and RBO72 (Figure 1b) to ~556 nm in RBO20 and RBO34. The long-wavelength shoulder peak at 605 nm in the absorption spectra of RBO*x* thin films is characteristic of the strong intermolecular interactions among chains of regioregular poly(3-alkylthiophene)s.[10] The photoluminescence spectra of RBO*x*, P3BT, and P3OT in toluene solutions all showed identical broad orange-red emission centered at 575−579 nm (Figure S2). We conclude that the photophysical properties of the random copoly(3-alkylthiophene)s are very similar to those of the poly(3-alkylthiophene)s, which is to be expected from the identical 2,5-linked polythiophene backbone and preservation of regioregularity in the random copolymers with multiple side chains.

Crystallinity of Random Copolythiophenes RBO*x*. The crystalline nature and the lamellar packing structure of the random copoly(3-alkylthiophene)s were investigated by differential scanning calorimetry (DSC) and X-ray diffraction (XRD). DSC scans of RBO*x* were performed in the range 0−270 °C under N_2 with a 10 °C/min heating/cooling rate, exemplified by the DSC scan of RBO50 shown in Figure 2a. The thermal transitions extracted from the second DSC scans are summarized in Table 1. Each RBO*x* showed a clear single melting transition (T_m) ranging from 196.1 °C in RBO20 to 216.0 °C in RBO50. The T_m is observed to increase with increasing composition *x* (mol % 3BT) of RBO*x* as shown in Figure 2b. The T_m dependence on composition is almost linear except for the RBO50 data point which is higher than the linear trend, likely due to its slightly higher regioregularity compared to the rest of RBO*x*. The T_m values of RBO*x* samples are generally in between the T_m of P3OT (190−200 °C) and P3BT (243−272 °C).[1a,13] It is known that the regioregular P3ATs show a higher T_m as the alkyl side chain length decreases.[1a] The observed increase of T_m with increasing molar composition of the 3BT units in the random copolymers RBO*x* is in line with this expectation. The observed melting enthalpy (ΔH_m) of RBO*x* is in a narrow

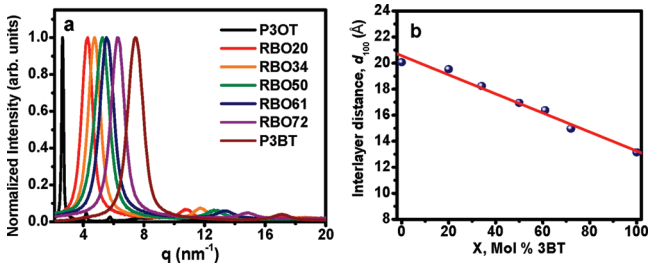

Figure 3. (a) XRD spectra of five RBO*x* copolymers, P3BT, and P3OT. (b) Compositional dependence of the interlayer stacking distance in RBO*x* copolymers.

range of 13.0−15.7 J/g (Table 1). These values are very similar to previously reported ΔH_m values (12−17 J/g) for P3BT, P3HT, and P3OT.[13d,e] The observed melting transition with a large enthalpy in the random copoly(3-alkylthiophene)s RBO*x* is strong evidence of crystalline morphology, similar to poly(3-alkylthiophene)s.[13] The exothermic recrystallization peak (T_c) following the melting in the RBO*x* samples was in the range 159.8−174.9 °C (Table 1). Similar to the linear trend of T_m discussed above, the T_c increases with increasing amount of the 3BT units in the random copolymer (Figure 2b).

The DSC results on RBO*x* provide important insights into the melting and crystallization behavior of poly(3-alkylthiophene)s, copoly(3-alkylthiophene)s and other conjugated polymers with side chains (Chart 1). First, the results mean that crystallization occurs in spite of the statistical distribution of side chains of significantly different sizes. This thus identifies RBO*x* as a new class of random copolymers that crystallizes. Second, the observed linear dependence of T_m and T_c on copolymer composition over the entire composition is very different from the known behavior of crystalline random copolymers of conventional nonconjugated polymers.[24] Crystallinity is rarely observed in the middle region of composition, especially the mid point of 50 mol %.[24] Third, we note that the copolymer composition variable provides a means of fine-tuning the thermal transition properties of the copoly(3-alkylthiophene)s in a continuous fashion not possible with conventional P3AT homopolymers.

To further confirm the crystalline nature of the random copolythiophenes we performed X-ray diffraction on drop-cast films of RBO*x* samples on glass substrates. The normalized XRD spectra of drop-cast films of RBO*x*, P3BT, and P3OT are shown in Figure 3a. Each polymer shows a similar diffraction pattern, consisting of a strong (100) reflection peak at *q* factor of 2.63−7.44 nm^{-1} (2θ angle of 4.4−6.74°) and a second weak peak at *q* factor of 4.20−17.10 nm^{-1} (2θ = 8.82−13.61°) due to the (200) reflection. Clearly, the random copolythiophenes RBO*x* have a lamellar crystalline structure similar to that of P3ATs. As the composition (mol % 3BT) of RBO*x* increases from RBO20 to RBO72, both the (100) and (200) peaks gradually shift to higher *q* values, meaning that the interlayer d_{100} spacing is decreasing. The compositional dependence of the d_{100} spacing of the lamellar crystalline structure of the random copolythiophenes RBO*x* along with those of the P3BT and P3OT is shown in Figure 3b. An excellent linear relationship, $d_{100}(x) = 20.07-0.0659x$, is obtained over the entire composition range ($0 \le x \le 100$). For example, d_{100} varies from 19.5 Å in RBO20 to 15.0 Å in RBO72, which are to be compared to 20.07 Å in P3OT and 13.14 Å in P3BT. The reported d_{100} values include 20.05−20.10 Å in P3OT and 12.63−12.80 Å in P3BT.[1a,13c] The full width at half-maximum (fwhm) of all

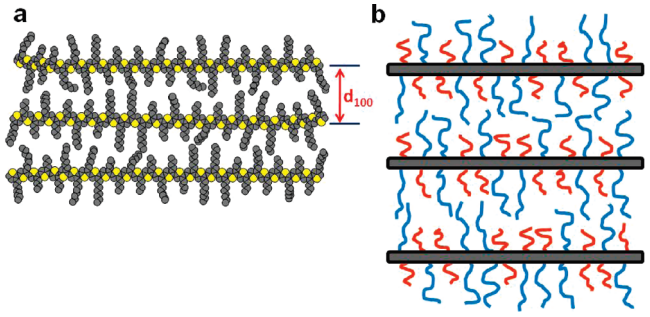

Figure 4. (a) Self-organization of random copolythiophenes RBO*x* into a lamellar crystalline structure. (b) Lamellar crystalline structure of random conjugated copolymers with different-sized side chains.

XRD diffraction signals and the corresponding crystallite sizes, calculated using the Scherrer equation,[25a] are summarized in Table S1 (Supporting Information). The sizes of the crystalline domains of RBO*x* are 11.5−14.3 nm, compared to 19.0 nm in P3OT and 11.2 nm in P3BT. Crystallites in P3HT films were found to be 12.2−15.9 nm, depending on the annealing temperature.[25b] The peak broadening of the (100) reflection of RBO*x* compared to that of P3OT is primarily due to the smaller crystallite size in RBO*x*. However, nonuniform microstrain may also contribute to the peak broadening in the cases of RBO50 and RBO61, where the slope values were much larger than that of P3OT as shown in Table S1 (Supporting Information).

The DSC and X-ray diffraction results allow us to conclude that macromolecular chains of these random copolythiophenes with statistical distribution of side chains of different sizes do self-organize into lamellar crystalline structures. A schematic model of such an assembly is shown in Figure 4a, which defines an interlayer stacking distance d_{100} that is continuously tuned by the random copolymer composition x. In spite of the considerable disorder in the local self-organization of the different-sized side chains within the interlayer space between copolymer backbones, nonarithmetic average intermolecular interaction distance is achieved at each composition which facilitates long-range crystalline order. In contrast to a single melting transition and a single (100) reflection peak observed in these random copolythiophenes RBO*x*, diblock copolythiophenes are reported to exhibit two distinct (100) reflections and two separate melting transitions due to their different segments.[20b] Similarly, it is known that binary blends of P3ATs have two different melting transitions in DSC scans if there is a significant difference (> 2 carbons) in the length of their side chains.[26] We expect that in general, conjugated copolymers with randomly distributed multiple-sized side chains can similarly self-organize into lamellar crystalline structures as illustrated in Figure 4b. The random copolymer composition in this case can provide a facile means of fine-tuning the lamellar crystalline structure and thus physical properties of conjugated polymers from two existing monomers. Regarding the two models of how the side chains of periodic conjugated polymers are organized,[16,17] our results suggest that both have validity and applicability to different polymers.

Photovoltaic and Charge Transport Properties. We have investigated the photovoltaic properties of the random copolythiophenes in bulk heterojunction (BHJ) solar cells in comparison with the two parent homopolymers (P3BT and P3OT) as well as with corresponding P3BT/P3OT physical blends. To gain insights into the BHJ solar cells the charge transport was also investigated by space charge limited current (SCLC) measurement and the morphology of the BHJ layer (polymer:$PC_{71}BM$) was investigated by TEM imaging.

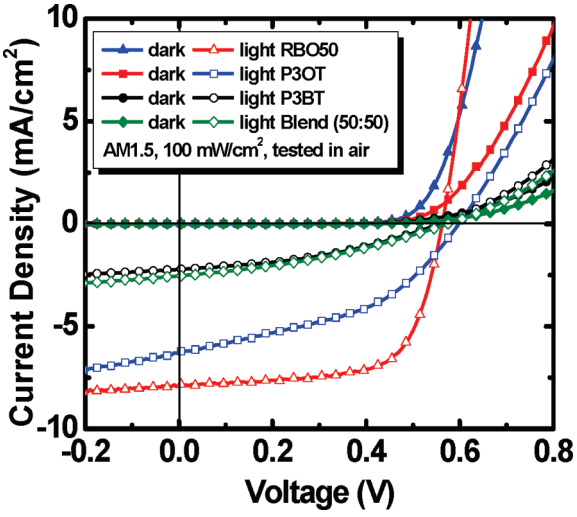

Figure 5. Current density−voltage characteristics of photovoltaic devices under 100 mW/cm^2 AM1.5 solar irradiation: RBO50:$PC_{71}BM$ (1:0.75), P3BT:$PC_{71}BM$ (1:0.75), P3OT:$PC_{71}BM$ (1:0.75), and 50% P3BT/P3OT blend:$PC_{71}BM$ (1:0.75).

Table 2. Photovoltaic Parameters of RBO*x*:$PC_{71}BM$, P3BT:$PC_{71}BM$, and P3OT:$PC_{71}BM$ BHJ Solar Cells and SCLC Mobility of Holes in the Devices

polymer	μ_h (cm^2/V s)	J_{sc} (mA/cm^2)	V_{oc} (V)	FF	PCE_{max} (%)	PCE_{ave} (%)
P3OT	3.2×10^{-4}	6.30	0.60	0.44	1.7	1.3
RBO20	4.1×10^{-5}	7.27	0.56	0.59	2.4	2.3
RBO34	2.1×10^{-5}	7.01	0.55	0.54	2.1	2.0
RBO50	1.8×10^{-4}	7.92	0.56	0.67	3.0	2.7
RBO61	2.1×10^{-4}	7.00	0.62	0.65	2.8	2.6
RBO72	1.3×10^{-5}	6.22	0.64	0.62	2.5	2.1
P3BT	4.2×10^{-7}	2.23	0.56	0.38	0.5	0.5

Representative current density (J) vs voltage (V) curves for BHJ solar cells based on RBO50, P3BT, P3OT, and the 50% P3BT/P3OT blend are shown in Figure 5. The photovoltaic parameters derived from the $J-V$ characteristics in Figure 5 and similar plots for the remaining RBO*x*:$PC_{71}BM$ BHJ devices, including the short-circuit current density (J_{sc}), open circuit voltage (V_{oc}), fill factor (FF), and power conversion efficiency (PCE) are summarized in Table 2. Similar J_{sc}, V_{oc}, FF, and PCE data for the BHJ devices from the P3BT/P3OT physical blends are collected in Table S2 (Supporting Information). Both J_{sc} and FF are significantly improved in RBO50:$PC_{71}BM$ solar cells compared to the related homopolymer (P3BT and P3OT) or P3BT/P3OT blend (50%) devices. RBO50:$PC_{71}BM$ solar cells gave the best photovoltaic performance of 3.0% PCE with a J_{sc} of 7.92 mA/cm^2, V_{oc} of 0.56 V, and FF of 0.67. The observed efficiency of RBO50 solar cells (3.0% PCE) represents factors of 6 and 1.8 enhancements compared to the homopolymers (P3BT, P3OT). A similarly large enhancement (~6×) was observed in RBO50 solar cells compared to the P3BT/P3OT blend (50%) devices. We note that solar cells based on P3OT, RBO20, and RBO34 gave higher efficiencies when the devices were dried at 60 °C for 2 h compared to the devices processed by 30 min film aging and 5 min thermal annealing at 110 ± 10 °C. Although a detailed understanding of the mechanism for enhancement of the photovoltaic properties of the random copolymers is yet to emerge, especially why the photovoltaic efficiency peaks at the symmetric composition (50%), it appears that the average interlayer distance in

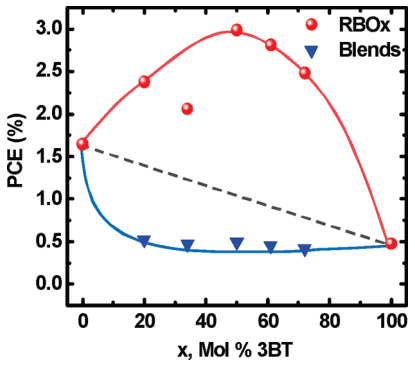

Figure 6. Compositional dependence of the power conversion efficiency of solar cells made from RBO*x*:$PC_{71}BM$ and P3BT/P3OT blend:$PC_{71}BM$ devices.

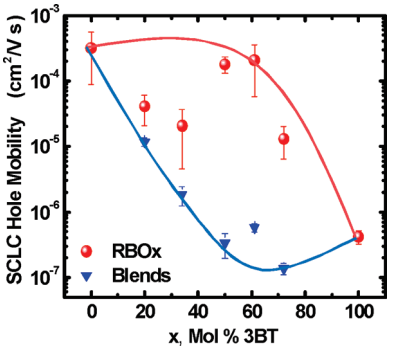

Figure 7. Compositional dependence of the SCLC mobility of holes in RBO*x*:$PC_{71}BM$ (1:0.75) blends and P3BT/P3OT:$PC_{71}BM$ (1:0.75) blends.

RBO50 provides one possible explanation. At 1.69 nm, the d_{100} spacing in RBO50 which is very close to that of P3HT (1.65 nm),[1a,13c] which is considered as a good p-type semiconductor with an optimal *d*-spacing that allows a reasonable degree of polymer/fullerene phase separation and diffusion of PCBM molecules while maximizing efficient charge transport in both donor/acceptor phases and the volume density of light absorbing backbone that leads to a higher photocurrent.

The observed open circuit voltage in all the RBO*x*:$PC_{71}BM$ BHJ devices is in the range of 0.56−0.64 V, and is comparable to those of P3BT (0.56 V) and P3OT (0.60 V). The short-current density of the RBO*x* solar cells is enhanced compared to the homopolymer devices (Table 2). The fill factor of the BHJ devices based on the random copolythiophenes was significantly higher compared with devices based on the homopolymers (P3BT and P3OT). The improvements in both J_{sc} and FF together result in the observed large enhancement in the efficiency of the RBO*x*:$PC_{71}BM$ solar cells. The compositional dependence of the efficiency of BHJ devices based on the random copolythiophenes RBO*x* is shown in Figure 6. Most notable is the nonlinear dependence of the power conversion efficiency on composition, showing that the RBO*x*-based BHJ solar cells outperform those of the homopolymers. We note that the efficiency (1.3−1.7% PCE) of the P3OT:$PC_{71}BM$ solar cells reported here is the highest reported to date for this homopolymer and is to be compared to the previous report of 0.45% PCE.[25a] The efficiency of ∼0.5% PCE observed here for P3BT:$PC_{71}BM$ BHJ devices compares favorably with prior reports for this polymer.[27a,b] However, more recent P3BT BHJ solar cells based on different processing strategies, such as self-assembled P3BT nanowires,[28] have resulted in efficiencies as high as 3.0−3.2% PCE.[28,29] Nevertheless, the observed compositional dependence of the efficiency of BHJ solar cells based on RBO*x* demonstrates that the photovoltaic properties of the random copolythiophenes are unexpectedly high and enhanced relative to the homopolymers. These random copolymers, RBO*x*, thus avoid the disadvantages of the poor processability of P3BT and the long alkyl side chains of P3OT.

The efficiency of BHJ solar cells based on $PC_{71}BM$ acceptor and P3BT/P3OT physical blends as donors is also shown in Figure 6 as a function of composition. The related photovoltaic parameters are given in Table S2 (Supporting Information). The photovoltaic efficiency of the P3BT/P3OT physical blends is seen to be independent of composition (Figure 6, Table S2), the numerical value (∼0.3−0.5% PCE) appears to be largely determined by the poorer of the two polymer blend components. Most importantly, we see that compared to the P3BT/P3OT physical blends the BHJ solar cells based on the random copolythiophenes are substantially enhanced (Figure 6).

The charge transport properties of the random copolymers RBO*x* and those of the homopolymers (P3BT, P3OT) and P3BT/P3OT physical blends were evaluated in space-charge limited current (SCLC) experiments using hole-only devices: ITO/PEDOT:PSS/active layer/Au, where the active layer is a polymer:$PC_{71}BM$ BHJ thin film processed under the same conditions as the solar cells. The dark-current density (*J*) − voltage (*V*) characteristics of the RBO*x*:$PC_{71}BM$ and P3BT/P3OT blend:$PC_{71}BM$ devices were analyzed by using nonlinear least-squares fitting (Figure S5, Supporting Information) to the Mott-Gurney equation,[23] yielding the zero-field SCLC hole mobility (μ_h). The SCLC mobility of holes in RBO*x*:$PC_{71}BM$, P3BT:$PC_{71}BM$ and P3OT:$PC_{71}BM$ BHJ thin films are summarized in Table 2. The highest mobility of holes was observed in P3OT:$PC_{71}BM$ (1:0.75) BHJ thin films at 3.2×10^{-4} $cm^2/(V\ s)$. In contrast, a rather low hole mobility was observed in P3BT:$PC_{71}BM$ BHJ thin films (4.2×10^{-7} $cm^2/(V\ s)$) which may be due to the poor solubility, large polydispersity in molecular weight (PDI = 3.61), and poor crystallinity in blends with $PC_{71}BM$. The mobility of holes in RBO*x*:$PC_{71}BM$ BHJ thin films varies from 1.3×10^{-5} $cm^2/(V\ s)$ in RBO72:$PC_{71}BM$ to 2.1×10^{-4} $cm^2/(V\ s)$ in RBO61:$PC_{71}BM$ (Table 2). The compositional dependence of the SCLC hole mobility, $\mu(x)$, in RBO*x*:$PC_{71}BM$ and P3BT/P3OT blends:$PC_{71}BM$ thin films is shown in Figure 7. Charge transport is enhanced in the random copolythiophenes RBO*x* compared to tht P3BT homopolymer. The μ_h values of RBO50, RBO61 and RBO72 BHJ thin films are comparable to that of P3OT. The similarly measured SCLC mobility of holes in P3BT/P3OT blends is plotted as a function of composition in Figure 7. The hole mobility varies from 1.4×10^{-7} to 1.2×10^{-5} $cm^2/(V\ s)$ in the physical blends (Table S2, Supporting Information). The mobility of holes in the random copolythiophene BHJ thin films is enhanced compared to the corresponding physical blends over the entire composition. Random poly(3-methylthiophene-*co*-3-hexylthiophene)s have similarly been found to exhibit comparable or improved field-effect charge transport compared to their parent homopolymers[30a,b] while a random poly(3-hexylthiophene-*co*-3-octylthiophene) was found to exhibit enhanced field-effect charge transport compared to P3OT and P3HT/P3OT blends.

The morphology of the BHJ thin films in the photovoltaic devices was investigated by TEM imaging and representative images of the homopolymers (P3BT, P3OT), RBO50, and a 50% P3BT/P3OT blend are shown in Figure 8. The

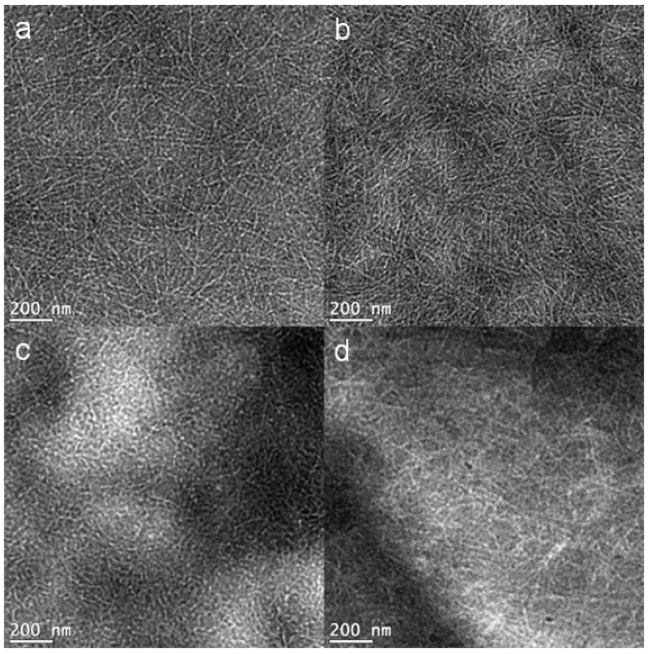

Figure 8. TEM images of $PC_{71}BM$ blend thin films: (a) P3BT, (b) P3OT, (c) RBO50, and (d) P3BT/P3OT blend (50%) under 200 kV.

morphology of BHJ films of P3BT is characterized by nanowires (NWs) of P3BT (Figure 8a) and absence of large-scale aggregation of $PC_{71}BM$. P3OT NWs dispersed in a $PC_{71}BM$ matrix with large and irregular dark areas indicative of the aggregation of $PC_{71}BM$ across the BHJ films are seen in the morphology of P3OT (Figure 8b). In contrast, the observed morphology of RBO50:$PC_{71}BM$ BHJ thin film (Figure 8c) and those of other random copolythiophene RBO*x*:$PC_{71}BM$ BHJ thin films consist of worm-like nanostructures. In the case of the physical blend BHJ thin film, a low density of polymer NWs and a large number of $PC_{71}BM$ aggregates in dark-shades area are observed in the TEM images (Figure 8d). The miscibility between the polymer donor and the $PC_{71}BM$ acceptor, the crystallization of the polymer and $PC_{71}BM$ phases, and the scale of the phase separation in the BHJ thin film are all critical to the overall performance of the bulk heterojunction solar cells. The observed differences in the morphology of the different BHJ thin films shown in Figure 8 could partly explain the photovoltaic performance of various BHJ solar cells. A previous report has indeed suggested that a random poly(3-dodecylthiophene-*co*-thiophene) had a better photovoltaic efficiency than the highly ordered poly(3,3‴-didodecylquaterthiophene) (PQT-12) because the former (random copolymer) more effectively mixed with the fullerene acceptor and formed bicontinuous networks with a nanoscale phase separation.[30d] BHJ thin films of PQT-12 were found by others to form nanoparticles with poor electrical connection in devices[31] due to the intercalation of fullerene molecules between side chains.[32]

The observed significant enhancement of photovoltaic power conversion efficiency in BHJ solar cells based on the random copoly(3-alkylthiophene)s relative to those of the homopolymers or physical blends can be understood in terms of many beneficial factors. In addition to their good solubility, which facilitates facile self-organization of the random copolythiophene (RBO*x*) chains into lamellar crystalline structures, high carrier mobility and a worm-like phase-separated network morphology of their BHJ thin films when blended with fullerene ($PC_{71}BM$) contribute to the improved photovoltaic properties. The engineered disordered interlayer space between the π-conjugated polymer backbones means that the present crystalline random copolymers must interact with fullerene molecules in novel ways compared to periodic conjugated polymers with uniform side chains such as P3ATs or PQT-12. Depending on the free volume between the side chains of a conjugated polymer, fullerene molecules can intercalate in fullerene: polymer BHJ thin films, which can influence the formation of ground state complexes and efficiency of the devices.[32] Unlike excited state complexes of a conjugated polymer which can be key intermediates in the exciton dissociation process,[33] it is unclear the formation of crystalline ground state complexes in fullerene/polymer systems[32] is advantageous. Multiple-sized side chains and random copolymerization offer a means to tune these intermolecular interactions.

Conclusions

We have synthesized and characterized new random copoly(3-alkylthiophene)s, poly(3-butylthiophene-*co*-3-octylthiophene) (RBO*x*). Our study of their structural properties by DSC and X-ray diffraction showed that the random copolythiophenes crystallize, melt, and form lamellar crystalline structures. Their melting and crystallization temperatures were found to vary continuously with copolymer composition. The interlayer stacking distance of the lamellar crystalline structure had a linear dependence on the composition of the random copolythiophenes. Fullerene-based bulk heterojunction (BHJ) solar cells fabricated from the random copolythiophenes were significantly enhanced compared to the homopolymers or physical blends. Enhanced charge transport and a more favorable nanoscale morphology of the BHJ thin films of the random copolythiophenes explain the improved photovoltaic properties. In general, these results demonstrate that random copoly(3-alkylthiophene)s with multiple-sized side chains represent a new class of crystalline random copolymers with readily tunable lamellar crystal lattice and electronic/optoelectronic properties.

Acknowledgment. Our report is based on research (polymer and organic/inorganic hybrid solar cells) supported by the U.S. DOE, Basic Energy Sciences, Division of Materials Science, under Award No. DE-FG02-07ER46467. S.A.J. also acknowledges the NSF (DMR-0805259 and DMR-0120967) for support of the synthesis of polymer semiconductors. G.R. received a fellowship award from the University of Washington, Center for Nanotechnology. Part of this work was conducted at the University of Washington NanoTech User Facility, a member of the NSF National Nanotechnology Infrastructure Network (NNIN).

Supporting Information Available: Figures showing ^1H NMR spectra, photoluminescence spectra, DSC data, XRD spectra, additional TEM images, and SCLC data of polymer thin films and tables giving structural parameters and photovoltaic parameters. This material is available free of charge via the Internet at http://pubs.acs.org.

References and Notes

(1) (a) Chen, T.-A.; Wu, X.; Rieke, R. D. *J. Am. Chem. Soc.* **1995**, *117*, 233–244. (b) Osaka, I.; McCullough, R. D. *Acc. Chem. Res.* **2008**, *41*, 1202–1214.
(2) Berresheim, A. J.; Müller, M.; Müllen, K. *Chem. Rev.* **1999**, *99*, 1747–1785.
(3) Suzuki, Y.; Hashimoto, K.; Tajima, K. *Macromolecules* **2007**, *40*, 6521–6528.
(4) (a) Bunz, U. H. F. *Chem. Rev.* **2000**, *100*, 1605–1644. (b) Egbe, D. A. M.; Carbonnier, B.; Birckner, E.; Grummt, U.-W. *Prog. Polym. Sci.* **2009**, *34*, 1023–1067.

(5) Rühe, J.; Ezquerra, T. A.; Wegner, G. *Synth. Met.* **1989**, *28*, 177–181.
(6) (a) Scherf, U.; List, E. J. W. *Adv. Mater.* **2002**, *14*, 477–487. (b) Neher, D. *Macromol. Rapid Commun.* **2001**, *22*, 1365–1385. (c) Leclerc, M. *J. Polym. Sci., Part A: Polym. Chem.* **2001**, *39*, 2867–2873.
(7) Blouin, N.; Leclerc, M. *Acc. Chem. Res.* **2008**, *41*, 1110–1119.
(8) (a) Zhu, Y.; Alam, M. M.; Jenekhe, S. A. *Macromolecules* **2002**, *35*, 9844–9846. (b) Zhu, Y.; Alam, M. M.; Jenekhe, S. A. *Macromolecules* **2003**, *36*, 8958–8968.
(9) (a) Kanbara, T.; Yamamoto, T. *Macromolecules* **1993**, *26*, 3464–3466. (b) Yamamoto, T.; Zhou, Z.-h.; Kanbara, T.; Shimura, M.; Kizu, K.; Maruyama, T.; Nakamura, Y.; Fukuda, T.; Lee, Bang-L.; Ooba, N.; Tomaru, S.; Kurihara, T.; Kaino, T.; Kubota, K.; Sasaki, S. *J. Am. Chem. Soc.* **1996**, *118*, 10389–10399. (c) Cui, Y.; Zhang, X.; Jenekhe, S. A. *Macromolecules* **1999**, *32*, 3824–3826.
(10) Hoeben, F. J. M.; Jonkheijm, P.; Meijer, E. W.; Schenning, A. P. H. J. *Chem. Rev.* **2005**, *105*, 1491–1546.
(11) Grimsdale, A. C.; Leok Chan, K.; Martin, R. E.; Jokisz, P. G.; Holmes, A. B. *Chem. Rev.* **2009**, *109*, 897–1091.
(12) (a) Yap, B. K.; Xia, R.; Campoy-Quiles, M.; Stavrinou, P. N.; Bradley, D. D. C. *Nat. Mater.* **2008**, *7*, 376–380. (b) Jenekhe, S. A. *Nat. Mater.* **2008**, *7*, 354–355.
(13) (a) Wu, P.-T.; Xin, H.; Kim, F. S.; Ren, G.; Jenekhe, S. A. *Macromolecules* **2009**, *42*, 8817–8826. (b) Babel, A.; Jenekhe, S. A. *Synth. Met.* **2005**, *148*, 169–173. (c) Samitsu, S.; Shimomura, T.; Heike, S.; Hashizume, T.; Ito, K. *Macromolecules* **2008**, *41*, 8000–8010. (d) Causin, V.; Marega, C.; Marigo, A.; Valentini, L.; Kenny, J. M. *Macromolecules* **2005**, *38*, 409–415. (e) Pal, S.; Roy, S.; Nandi, A. K. *J. Phys. Chem. B* **2005**, *109*, 18332–18341.
(14) (a) Mena-Osteriz, E.; Meyer, A.; Langeveld-Voss, B. M. W.; Janssen, R. A. J.; Meijer, E. W.; Bäuerle, P. *Angew. Chem., Int. Ed.* **2000**, *39*, 2679–2684. (b) Brinkmann, M.; Rannou, P. *Macromolecules* **2009**, *42*, 1125–1130.
(15) (a) Ong, B. S.; Wu, Y.; Liu, P.; Gardner, S. *J. Am. Chem. Soc.* **2004**, *126*, 3378–3379. (b) Ong, B. S.; Wu, Y.; Li, Y.; Liu, P.; Pan, H. *Chem.—Eur. J.* **2008**, *14*, 4766–4778.
(16) McCulloch, I.; Heeney, M.; Bailey, C.; Genevicius, K.; MacDonald, I.; Shkunov, M.; Sparrowe, D.; Tierney, S.; Wagner, R.; Zhang, W.; Chabinyc, M. L.; Kline, R. J.; McGehee, M. D.; Toney, M. F. *Nat. Mater.* **2006**, *5*, 328–333.
(17) Kline, R. J.; DeLongchamp, D. M.; Fischer, D. A.; Lin, E. K.; Richter, L. J.; Chabinyc, M. L.; Toney, M. F.; Heeney, M.; McCulloch, I. *Macromolecules* **2007**, *40*, 7960–7965.
(18) Osaka, I.; Zhang, R.; Sauvé, G.; Smilgies, D.-M.; Kowalewski, T.; McCullough, R. D. *J. Am. Chem. Soc.* **2009**, *131*, 2521–2529.
(19) Ahmed, E.; Kim, F. S.; Xin, H.; Jenekhe, S. A. *Macromolecules* **2009**, *42*, 8615–8618.
(20) (a) Iovu, M. C.; Sheina, E. E.; Gil, R. R.; McCullough, R. D. *Macromolecules* **2005**, *38*, 8649–8656. (b) Wu, P.-T.; Ren, G.; Li, C.; Mezzenga, R.; Jenekhe, S. A. *Macromolecules* **2009**, *42*, 2317–2320. (c) Ren, G.; Wu, P.-T.; Jenekhe, S. A. *Chem. Mater.* **2010**, *22*, 2020−2026.
(21) (a) Lowe, R. S.; Khersonsky, S. M.; McCullough, R. D. *Adv. Mater.* **1999**, *11*, 250–253. (b) Heeny, M.; Zhang, W.; Duffy, W.; McCulloch, I.; Koller, G. World Patent Application WO2007/059838, **2007**.
(22) Xin, H.; Guo, X.; Kim, F. S.; Ren, G.; Watson, M. D.; Jenekhe, S. A. *J. Mater. Chem.* **2009**, *19*, 5303–5310.
(23) (a) Murgatroyd, P. N. *J. Phys. D: Appl. Phys.* **1970**, *3*, 151–156. (b) Mihailetchi, V. D.; Xie, H.; de Boer, B.; Koster, L. J. A.; Blom, P. W. M. *Adv. Funct. Mater.* **2006**, *16*, 699–708.
(24) (a) Lu, X.; Windle, A. H. *Polymer* **1995**, *36*, 451–459. (b) Stagnaro, P.; Boragno, L.; Canetti, M.; Forlini, F.; Azzurri, F.; Alfonso, G. C. *Polymer* **2009**, *50*, 5242–5249.
(25) (a) Patterson, A. L. *Phys. Rev.* **1939**, *56*, 978–982. (b) Motaung, D. E.; Malgas, G. F.; Arendse, C. J.; Mavundla, S. E.; Oliphant, C. J.; Knoesen, D. *J. Mater. Sci.* **2009**, *44*, 3192–3197.
(26) Pal, S.; Nandi, A. K. *Macromolecules* **2003**, *36*, 8426–8432.
(27) (a) Nguyen, L. H.; Hoppe, H.; Erb, T.; Günes, S.; Gobsch, G.; Sariciftci, N. S. *Adv. Funct. Mater.* **2007**, *17*, 1071–1078. (b) Hiorns, R. C.; de Bettignies, R.; Leroy, J.; Bailly, S.; Firon, M.; Sentein, C.; Khoukh, A.; Preud'homme, H.; Dagron-Lartigau, C. *Adv. Funct. Mater.* **2006**, *16*, 2263–2273.
(28) (a) Xin, H.; Kim, F. S.; Jenekhe, S. A. *J. Am. Chem. Soc.* **2008**, *130*, 5424–5425. (b) Xin, H.; Ren, G.; Kim, F. S.; Jenekhe, S. A. *Chem. Mater.* **2008**, *20*, 6199–6207.
(29) Gadisa, A.; Oosterbaan, W. D.; Vandewal, K.; Bolsée, J.-C.; Bertho, S.; D'Haen, J.; Lutsen, L.; Vanderzande, D.; Manca, J. V. *Adv. Funct. Mater.* **2009**, *19*, 3300–3306.
(30) (a) Jackson, T.; Wang, J. U.S. Patent 6,621,098, **2003**. (b) Wang, J.; Gundlach, D. J.; Benesi, A. J.; Jackson, T. N. Abstract, 1999 Electronic Materials Conf., Santa Barbara, CA, June 30−July 2, 1999. (c) Zen, A.; Saphiannikova, M.; Neher, D.; Asawapirom, U.; Scherf, U. *Chem. Mater.* **2005**, *17*, 781–786. (d) Thompson, B. C.; Kim, B. J.; Kavulak, D. F.; Sivula, K.; Mauldin, C.; Fréchet, J. M. J. *Macromolecules* **2007**, *40*, 7425–7428.
(31) Moulé, A. J.; Allard, S.; Kronenberg, N. M.; Tsami, A.; Scherf, U.; Meerholz, K. *J. Phys. Chem. C* **2008**, *112*, 12583–12589.
(32) Mayer, A. C.; Toney, M. F.; Scully, S. R.; Rivnay, J.; Brabec, C. J.; Scharber, M.; Koppe, M.; Heeney, M.; McCulloch, I.; McGehee, M. D. *Adv. Funct. Mater.* **2009**, *19*, 1173–1179.
(33) (a) Jenekhe, S. A.; Osaheni, J. A. *Science* **1994**, *265*, 765–768. (b) Jenekhe, S. A. *Adv. Mater.* **1995**, *7*, 309–311.